

# OpenDPDv2: A Unified Learning and Optimization Framework for Neural Network Digital Predistortion

Yizhuo Wu<sup>✉</sup>, *Graduate Student Member*, Ang Li<sup>✉</sup>, *Graduate Student Member*, Chang Gao<sup>\*✉</sup>, *Member*

**Abstract**—Neural network (NN)-based Digital Predistortion (DPD) has demonstrated superior performance in improving signal quality in wideband radio frequency (RF) power amplifiers (PAs) employing complex modulation. However, NN DPDs usually rely on a large number of parameters for effective linearization and can significantly contribute to the energy consumption of the digital back-end in RF systems. This paper presents OpenDPDv2, an open-source, end-to-end framework that unifies PA modeling, NN-DPD learning, and deployment-oriented model optimization to reduce inference energy while preserving linearization performance. OpenDPDv2 introduces temporal residual (TRes)-Delta Gated Recurrent Unit (DeltaGRU), a delta-RNN DPD architecture with a lightweight temporal residual path that improves robustness under aggressive temporal sparsity, and it supports joint optimization of temporal sparsity and fixed-point quantization. On a 3.5 GHz GaN Doherty PA driven by a TM3.1a 200 MHz 256-QAM OFDM signal, the FP32 TRes-DeltaGRU model achieves Adjacent Channel Power Ratio (ACPR) of  $-59.9$  dBc and Error Vector Magnitude (EVM) of  $-42.1$  dB. By combining quantization with dynamic temporal sparsity, the model reduces inference energy by  $4.5\times$  while maintaining  $-51.8$  dBc ACPR and  $-35.2$  dB EVM at 56% temporal sparsity. Code, datasets, and documentation are publicly available at <https://github.com/lab-emi/OpenDPD>.

**Index Terms**—digital predistortion (DPD), temporal sparsity, power amplifier (PA), recurrent neural network (RNN), digital signal processing (DSP)

## I. INTRODUCTION

THE exponential growth of wireless data traffic has driven growing demands for broader spectrum usage, higher data rates, and fewer error occurrences in modern wireless communication systems. However, wideband Radio Frequency (RF) Power Amplifiers (PAs), as an essential component in TX systems, degrade the signal quality by inherent distortions. These distortions increase out-of-band emissions and degrade in-band signal quality, leading to higher EVM and symbol errors, negatively impacting both communication reliability and energy efficiency. To address these challenges, Digital Pre-distortion (DPD) has become a popular method.

DPD aims to derive an inverse function of PAs transfer function to compensate for nonlinearity before the signal passes through the RF transmitter. Conventional DPD methods based on Volterra-series deliver effective linearization in narrowband scenarios but struggle with wideband and high-constellation modulated signals to satisfy communication standards [1]. In contrast, Machine Learning (ML) techniques, such as Neural Network (NN)-based DPD,

outperform Generalized Memory Polynomial (GMP) model for Orthogonal Frequency Division Modulation (OFDM) signal with bandwidth higher than 200 MHz and meet the requirement of communication standard [2]–[5].

However, the DPD module consumes a substantial portion of power in wideband radio digital back-ends [6]. The incorporation of Neural Networks (NNs) could further intensify this power issue. This high power consumption in digital signal processors runs counter to the goal of energy-efficient wideband transmitters in base stations and Wi-Fi access points, where the power budget is tight.

Previous approaches to reduce DPD energy consumption include lowering the sample rate [7], employing a sub-Nyquist feedback receiver in the observation path [8], dynamically adjusting model cross-terms based on input signal characteristics [9], simplifying computational pathways for DPD algorithms [10], and pruning less critical weights in fully connected layers to achieve static spatial weight sparsity [11].

This article presents OpenDPDv2, a unified open-source NN-based DPD framework for accurate PA modeling, DPD learning, and in-situ model optimization towards reduced arithmetic operations and energy-expensive memory accesses, and goes beyond our previous works [12]–[15]. While our prior publications introduced DeltaDPD and quantization-aware DPD learning as foundational techniques, they suffered from several limitations: (i) the DeltaGRU output sparsity was directly coupled to hidden state sparsity, limiting achievable temporal sparsity without dramatically decreasing the linearization performance; (ii) energy evaluations relied on idealized theoretical calculations that may not reflect practical processor behaviors; and (iii) temporal sparsity and quantization were optimized separately, missing potential synergies. This journal paper addresses these limitations by introducing a TCN-based residual path that decouples output from hidden state sparsity, providing realistic energy estimates using Gem5 simulation, and presenting a unified training framework that jointly optimizes both techniques.

The main contributions are:

- 1) **TRes-DeltaGRU: a new delta-RNN DPD architecture with robust wideband linearization under temporal sparsity.** We propose TRes-DeltaGRU, which introduces a Temporal Convolutional Networks (TCN)-based temporal residual path to decouple output dynamics from hidden-state sparsity, improving robustness at aggressive delta thresholds. With a 200 MHz TM3.1a 256-QAM OFDM signal on a 3.5 GHz GaN Doherty Power Amplifier (PA) at 41.2 dBm average

<sup>\*</sup>Corresponding author: Chang Gao (chang.gao@tudelft.nl)  
Yizhuo Wu, Ang Li, and Chang Gao are with the Department of Microelectronics, Delft University of Technology, The Netherlands.

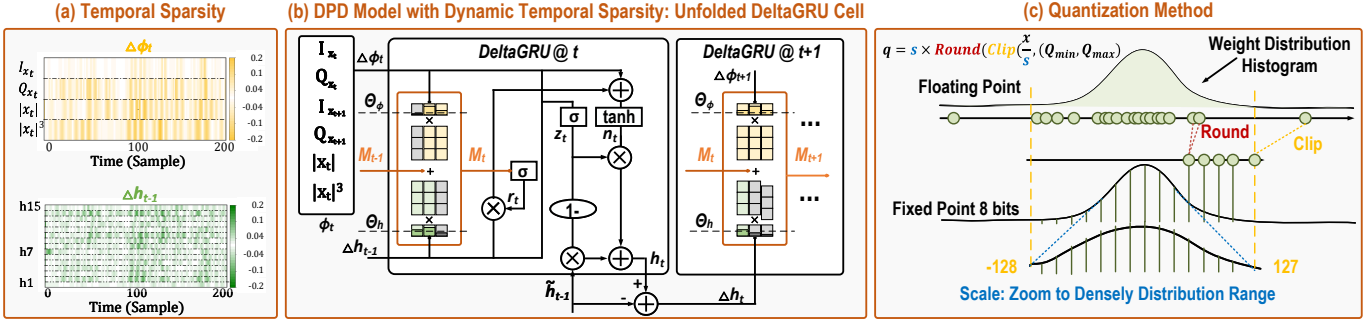


Fig. 1. (a) Dynamic temporal sparsity in recurrent neural network-based DPD input and hidden neurons. (b) Unfolded DeltaGRU Cell in DPD Model with temporal sparsity. (c) Quantization Method.

output power, the FP32 TRes-DeltaGRU-999 achieves measured linearization performance of -59.9 dBc ACPR and -42.1 dB EVM.

2) **OpenDPDv2: a reproducible end-to-end learning & optimization pipeline.** We release OpenDPDv2, a unified PyTorch-based framework that (i) trains DPD models end-to-end through a frozen PA surrogate and (ii) supports joint optimization with delta-threshold temporal sparsity and quantization-aware training; the framework includes the APA\_200MHz dataset and re-implemented baselines for reproducible head-to-head comparison.

3) **Realistic energy estimation on a practical processor model.** We present a power breakdown of NN-DPD operation across inference, sampling, adaptation, and provide realistic inference-energy estimates using Gem5 ARM CPU simulation with quantified instruction and cache-access statistics, showing how mixed precision and temporal sparsity translate into end-to-end energy reduction and revealing memory access as the dominant cost driver.

## II. FUNDAMENTALS

To model PA distortions with memory effects accurately, prior state-of-the-art approaches have predominantly employed Recurrent Neural Network (RNN)-based models, along with advanced feature extraction techniques. Feature extraction methods driven by PA behavior and signal configuration characteristics, such as Phase Gated (PG) [2], Decomposed Vector Rotation (DVR) [3], Block-oriented (BO) [5], and Phase Normalization (PN) [4], enable RNN-based models to achieve better linearization performance with fewer model parameters. However, DPD models still typically require 500-1000 parameters to stably satisfy communication standards at bandwidths above 200 MHz. Beyond structural optimization, we explore two complementary directions for energy reduction in our prior works: (i) exploiting dynamic temporal sparsity in RNN-based DPD [14], and (ii) applying mixed-precision arithmetic via quantization-aware DPD learning [13]. While mixed precision reduces the cost of MAC operations and memory access, temporal sparsity reduces the frequency of these operations. In our prior works, we introduced the Delta network algorithm and

mixed-precision DPD on top of high-accuracy dense models, which form the foundation of this work.

### A. Delta Network Algorithm

We exploit intrinsic temporal sparsity in I/Q signals and neural DPD model states using the delta network algorithm [16]. We consider the input feature set  $[I_{xt}, Q_{xt}, |x_t|, |x_t|^3]$  as an example. For continuous sequential signals, the element-wise changes between consecutive time steps ( $\Delta$ ) in the input neurons  $\Delta\phi$  and hidden states  $\Delta h$  are visualized in Figure 1 (a). The Delta maps in Figure 1 (a) are obtained from a 200MHz OFDM signal and a 15-neuron hidden-state vector from our proposed Gated Recurrent Unit (GRU)-based DPD model. White pixels indicate Delta values close to zero, revealing strong temporal redundancy over time. This temporal stability in both  $\Delta\phi$  and  $\Delta h$  enables transforming dense-matrix-dense-vector multiplication ( $\mathbf{M} \times \mathbf{V}$ ) into dense-matrix-sparse-vector multiplication ( $\mathbf{M} \times \mathbf{S}\mathbf{V}$ ).

In the Delta network algorithm, the sequential  $\mathbf{M} \times \mathbf{V}$  operation is rewritten as an incremental update driven by temporal differences:

$$\mathbf{y}_t = \mathbf{W}\mathbf{v}_t, \quad (1)$$

$$\mathbf{y}_t = \mathbf{W}\Delta\mathbf{v}_t + \mathbf{y}_{t-1} = \mathbf{W}(\mathbf{v}_t - \mathbf{v}_{t-1}) + \mathbf{y}_{t-1}, \quad (2)$$

Here,  $\mathbf{v}_t$  denotes either the RNN input  $\phi_t$  or the hidden state  $\mathbf{h}_{t-1}$ . We sparsify  $\Delta\mathbf{v}_t$  using a threshold  $\Theta_v$ , retaining only elements with meaningful changes:

$$\Delta\mathbf{v}_t = \begin{cases} \mathbf{v}_t - \tilde{\mathbf{v}}_{t-1}, & |\mathbf{v}_t - \tilde{\mathbf{v}}_{t-1}| > \Theta_v, \\ 0, & |\mathbf{v}_t - \tilde{\mathbf{v}}_{t-1}| \leq \Theta_v, \end{cases} \quad (3)$$

where  $\tilde{\mathbf{v}}$  is a memory buffer that stores the latest effective value. For the  $k$ -th element, the buffer is updated only when the change surpasses the threshold:

$$\tilde{v}_{t-1}^k = \begin{cases} v_{t-1}^k, & |v_t^k - \tilde{v}_{t-1}^k| > \Theta_v, \\ \tilde{v}_{t-2}^k, & |v_t^k - \tilde{v}_{t-1}^k| \leq \Theta_v. \end{cases} \quad (4)$$

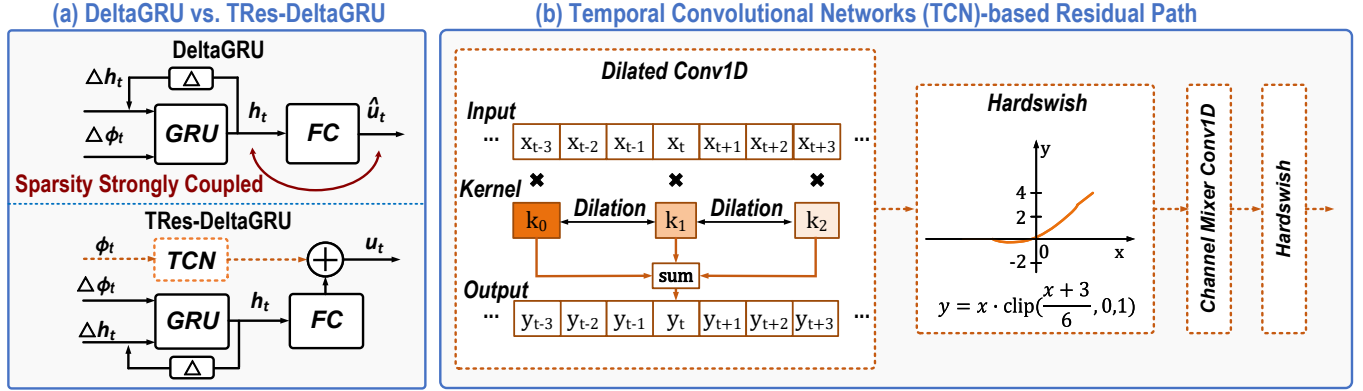


Fig. 2. (a) Comparison between DeltaGRU and TRes-DeltaGRU. (b) The architecture of Temporal Convolutional Networks-based Residual Path.

The delta formulation of the GRU update can be expressed as:

$$\mathbf{r}_t = \sigma(\mathbf{M}_{r,t}), \quad (5)$$

$$\mathbf{z}_t = \sigma(\mathbf{M}_{z,t}), \quad (6)$$

$$\mathbf{n}_t = \tanh(\mathbf{M}_{n\phi,t} + \mathbf{r}_t \odot \mathbf{M}_{nh,t}), \quad (7)$$

$$\mathbf{h}_t = (1 - \mathbf{z}_t) \odot \mathbf{h}_{t-1} + \mathbf{z}_t \odot \mathbf{n}_t. \quad (8)$$

The terms  $\mathbf{M}_{r,t}$ ,  $\mathbf{M}_{z,t}$ ,  $\mathbf{M}_{n\phi,t}$ , and  $\mathbf{M}_{nh,t}$  are the pre-activation accumulators, initialized by  $\mathbf{M}_{r,0} = \mathbf{b}_{ir} + \mathbf{b}_{hr}$ ,  $\mathbf{M}_{z,0} = \mathbf{b}_{iz} + \mathbf{b}_{hz}$ ,  $\mathbf{M}_{n\phi,0} = \mathbf{b}_{in}$ ,  $\mathbf{M}_{nh,0} = \mathbf{b}_{hn}$ , and updated incrementally as:

$$\mathbf{M}_{r,t} = \mathbf{W}_{ir}\Delta\phi_t + \mathbf{W}_{hr}\Delta\mathbf{h}_{t-1} + \mathbf{M}_{r,t-1}, \quad (9)$$

$$\mathbf{M}_{z,t} = \mathbf{W}_{iz}\Delta\phi_t + \mathbf{W}_{hz}\Delta\mathbf{h}_{t-1} + \mathbf{M}_{z,t-1}, \quad (10)$$

$$\mathbf{M}_{n\phi,t} = \mathbf{W}_{in}\Delta\phi_t + \mathbf{M}_{n\phi,t-1}, \quad (11)$$

$$\mathbf{M}_{nh,t} = \mathbf{W}_{hn}\Delta\mathbf{h}_{t-1} + \mathbf{M}_{nh,t-1}. \quad (12)$$

The schematic of the unfolded DeltaGRU Cell over time is illustrated in Fig. 1 (b). Temporal Residual Delta Gated Recurrent Unit (TRes-DeltaGRU) approach employs Delta thresholds  $\Theta_\phi$  and  $\Theta_h$  to bypass multiply-accumulate (MAC) operations and memory accesses associated with  $\Delta$  vector elements below these thresholds, along with their corresponding weight columns.

In the GRU block of Fig. 1 (b), all gray elements represent those skipped during processing. The predicted DPD output is generated by a final Fully-Connected (FC) layer:

$$\hat{\mathbf{u}}_t = \mathbf{W}_{\hat{y}}\mathbf{h}_t + \mathbf{b}_{\hat{y}}. \quad (13)$$

### B. Quantization-Aware DPD Learning

[17] and [18] show that **INT8** MAC operations can be up to  $20\times$  more energy efficient than **FP32** MAC operations (e.g., in 45 nm and 7 nm technology nodes). While 32-bit floating-point (**FP32**) arithmetic improves numerical precision, it increases inference energy  $E_{\text{INF}}$  and reduces energy efficiency. These results motivate quantization-aware DPD learning, where low-precision fixed-point arithmetic is used to reduce both computation and memory access with minimal performance loss.

Fig. 1 (c) clarifies that the quantization process from floating-point data  $x$  to fixed-point representation  $q$  is computed as:

$$q = s \times \text{Round} \left( \text{Clip} \left( \frac{x}{s}, Q_{\min}, Q_{\max} \right) \right) \quad (14)$$

where  $s$  is the quantization scale and  $[Q_{\min}, Q_{\max}]$  defines the  $n$ -bit integer range. The `Clip` function bounds  $x/s$  to  $[Q_{\min}, Q_{\max}]$ , with  $Q_{\min} = -2^{n-1}$  and  $Q_{\max} = 2^{n-1} - 1$  for signed quantization, and `Round` maps the result to the nearest integer. During training,  $s$  is learned per layer via gradient descent and constrained to the nearest power of two to support efficient fixed-point implementation.

## III. PROPOSED TRES-DELTAGRU

### A. Analysis of RNN and DPD Output

In the initial version of DeltaGRU, the GRU layer processes the input feature and its memory effect with a recurrent structure. The predicted DPD outputs are generated by a final FC layer as Equation 13. However, with this output layer, the sparsity of the pre-distorted DPD output  $\hat{\mathbf{u}}_t$  is directly coupled to the sparsity of the hidden state  $\mathbf{h}_t$ .

We take  $\Theta_h = 0.05$  as an example. At  $\Theta_h = 0.05$ , the relative sparsity of  $\mathbf{h}_t$  with respect to this threshold is as high as 81.8%. However, the actual sparsity of the PA output with respect to this threshold is only 42.4%. Directly correlating  $\mathbf{h}_t$  and  $\hat{\mathbf{u}}_t$  limits the magnitude of changes between consecutive points in the DPD output, resulting in a loss of accuracy.

### B. TRes-DeltaGRU Algorithm

To address this dependency, we introduce a residual connection between the input and output layers. We employ a TCN as the residual path to balance efficiency and performance, as detailed in Figure 2 (a).

The core of the TCN is dilated convolutions, which perform convolution on neighboring parameters in the convolutional kernel at intervals of  $D$ , rather than on consecutive time points of the input, as illustrated in Figure 2 (b). This approach expands the receptive field of a Convolutional Neural Network (CNN) with a kernel size of  $K$  from  $K$  to  $(K-1) \times D + 1$  without increasing the parameter count. Additionally, dilated

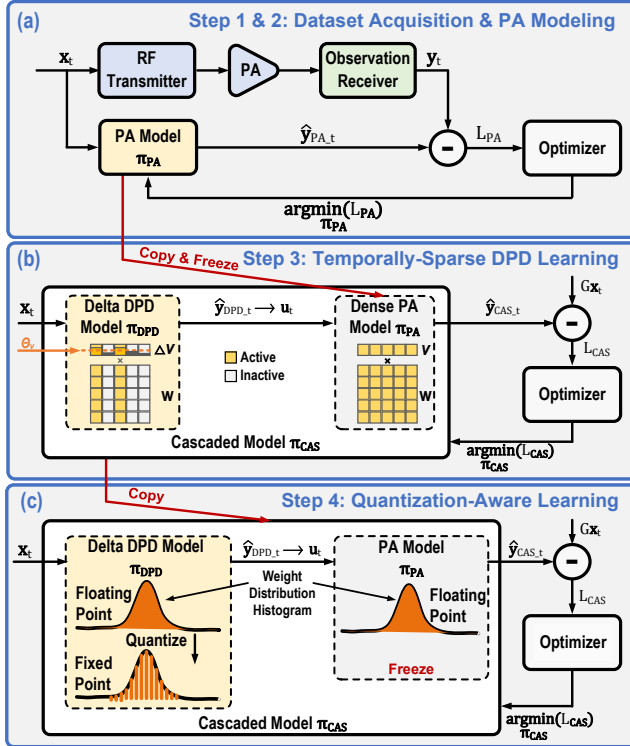


Fig. 3. Learning and optimization flow of OpenDPDv2.

convolution samples the input at a larger temporal stride within the kernel (without reducing the input sampling rate), enabling the residual path to capture a wider temporal context and improving EVM. The TCN residual path is defined as:

$$\text{TCN} = [\text{Dilated Conv1D}, \text{Hardswish}, \text{Conv1D}, \text{Hardswish}] \quad (15)$$

where the Hardswish activation function is:

$$y = x \cdot \text{clip}\left(\frac{x+3}{6}, 0, 1\right) \quad (16)$$

The Hardswish activation function provides smooth gradients around zero that facilitate training, and maintains non-linearity while being more hardware-friendly than traditional activation functions like ReLU, making it suitable for efficient DPD implementations.

The final output of the DPD module,  $\mathbf{U}$ , is expressed as:

$$[\mathbf{I}_u, \mathbf{Q}_u] = \mathbf{U} = \hat{\mathbf{U}} + \text{TCN}(\mathbf{X}) \quad (17)$$

where  $\hat{\mathbf{U}} = \{\hat{\mathbf{u}}_t | \hat{\mathbf{u}}_t = \mathbf{W}_{\hat{y}} \mathbf{h}_t + \mathbf{b}_{\hat{y}}, \mathbf{h}_t \in \mathbb{R}^H, t \in 0, \dots, T-1\}$ .  $H$  is the hidden size of DeltaGRU.

#### IV. OPENDPDV2

Building upon the proposed methods, we introduce OpenDPDv2, an enhanced version of our open-source, end-to-end (E2E) learning framework. The term "end-to-end" refers to a learning paradigm where the entire system, from raw input to final output, is trained as a unified pipeline in a single optimization process, rather than training

individual components separately and then combining them. This approach enables gradients to flow directly from the final linearization performance back through all system components, allowing for joint optimization that accounts for interactions between modules. In our framework, E2E training is achieved by cascading the DPD model with a pre-trained, frozen PA surrogate model and optimizing the DPD parameters using a loss defined at the PA output. OpenDPDv2 extends OpenDPDv1 [12] with the new TRes-DeltaGRU algorithm, two optimization methodologies, including temporal sparsity through delta threshold mechanisms and quantization-aware training for hardware-efficient deployment.

As depicted in Fig. 3, the architecture of OpenDPDv2 comprises four primary steps. Steps 1 and 2 maintain the foundational framework of OpenDPDv1, while steps 3 and 4 introduce the temporal sparse DPD learning and quantization-aware learning methodologies:

- **Step 1 & 2: Data Acquisition & PA Modeling (Fig. 3a):** The baseband input I/Q signal is represented as  $\mathbf{X} = \{\mathbf{x}_t | \mathbf{x}_t = I_{x_t} + jQ_{x_t}, I_{x_t}, Q_{x_t} \in \mathbb{R}, t \in 0, \dots, T-1\}$ . Transmitting it through the PA, the baseband output signals are captured as  $\mathbf{Y} = \{\mathbf{y}_t | \mathbf{y}_t = I_{y_t} + jQ_{y_t}, I_{y_t}, Q_{y_t} \in \mathbb{R}, t \in 0, \dots, T-1\}$ . A behavioral PA model,  $\pi_{PA}$ , is trained via BackPropagation Through Time (BPTT) to minimize the Mean Square Error (MSE) between predicted  $\hat{\mathbf{y}}_{PA}[n]$  and ground truth PA output  $\mathbf{y}[n]$ .
- **Step 3: Temporally-Sparse DPD Learning (Fig. 3b):** Building upon the DPD learning step of OpenDPDv1, OpenDPDv2 introduces the TRes-DeltaGRU algorithm with Delta threshold mechanisms. The Delta NN-based DPD model employs temporal sparsity through delta thresholds  $\Theta_\phi$  and  $\Theta_h$  to achieve computational efficiency. The DPD model with dynamic temporal sparsity  $\pi_{DPD}$  is cascaded before the pre-trained, frozen  $\pi_{PA}$ , to form the cascaded model  $\pi_{CAS}$ . Using BPTT,  $\pi_{CAS}$  is trained to approximate a linear transfer function with  $\mathbf{x}[n]$  as input and  $G\mathbf{x}[n]$  as output, enabling  $\pi_{DPD}$  to learn the inverse of the PA behavior.
- **Step 4: Quantization-Aware Optimization (Fig. 3c):** OpenDPDv2 implements quantization-aware training as the fourth step [19] to optimize the TRes-DeltaGRU DPD model for hardware deployment. During training, full-precision variables are updated during gradient descent while quantized values are used in forward propagation. By integrating quantization into the DPD model with dynamic temporal sparsity, our framework further optimizes energy consumption while preserving DPD performance. The gradient of the Round function is approximated using the straight-through estimator [20] to ensure effective training.

#### V. EXPERIMENTAL SETUP

The key experimental parameters are summarized in Table I.

##### A. Measurement Setup

Figure 4 depicts the experimental setup utilized in this study. The OFDM baseband I/Q signal was generated by an

TABLE I  
EXPERIMENTAL SETUP PARAMETERS

Category	Parameter	Value
Measurement Equipment	Signal Generator	R&S-SMW200A
	Spectrum Analyzer	R&S-FSW43
	Resolution Bandwidth	100 Hz
	EVM Calculation	Input vs. digitized output
Test Signal	Signal Type	TM3.1a 5×40-MHz (200-MHz) 256-QAM
	PAPR	10.01 dB (at CCDF of 0.001%)
	Sampling Rate	983.04 MHz
	Dataset Size	98304 samples
	Train/Val/Test Split	60%/20%/20%
Power Amplifier (DUT)	Dataset Name	APA_200MHz
	Type	3.5 GHz GaN Doherty
	Average Output Power	41.2 dBm
	P1dB Compression Point	46.5 dBm
	P3dB Compression Point	50 dBm
Training Configuration	Flat Gain Bandwidth	200 MHz
	Platform	OpenDPDv2 (PyTorch 2.4.1)
	Epochs	240
	Optimizer	ADAMW
	Initial Learning Rate	5E-3
	Learning Rate Decay	ReduceOnPlateau
	Batch Size	64
	Hardware	NVIDIA RTX 4090 (CUDA 12.4)

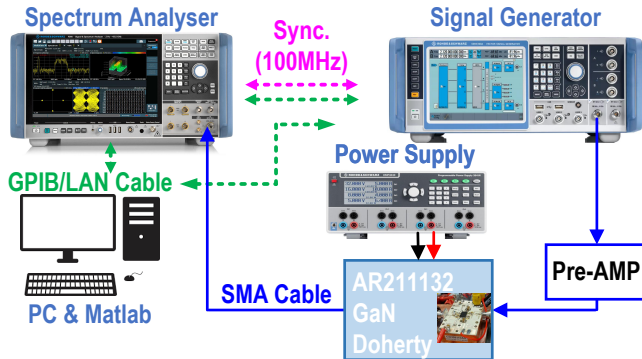


Fig. 4. Setup for dataset acquisition and DPD performance measurement.

R&S-SMW200A signal generator and amplified by a PA with the same average output power, with and without DPD. The resulting output signal was digitized using an R&S-FSW43 spectrum analyzer. During the ACPR measurements, the resolution bandwidth is set as 100 Hz to decrease the noise floor of the spectrum analyzer [21]. The EVM was computed by comparing the input signal with the digitized output signal instead of the reference grid.

#### B. Test Signals and Design-Under-Test (DUT)

The experiment employed APA\_200MHz, a TM3.1a 5×40-MHz (200-MHz) 256-QAM signal with a Peak-to-Average Power Ratio (PAPR) of 10.01 dB at Complementary Cumulative Distribution Function (CCDF) of

TABLE II  
COMPARISON OF NEURAL DPD MODELS TRAINED BY OPENDPDV2

Dense DPD Models	#Params	FLOPs <sup>a</sup>	NMSE (dB)	EVM (dB)	ACPR (dBc)
Without DPD	-	-	-20.5	-24.7 (5.84%)	-28.3
RVTDCNN [22]	1007	1587 (+23.8%)	-32.9	-33.9 (2.03%)	-50.8
PG-JANET [2]	1130	1507 (+17.6%)	-36.6	-39.3 (1.09%)	-58.2
DVR-JANET [3]	1097	1370 (+6.9%)	-37.0	-38.6 (1.17%)	-59.4
BO-JANET [5]	1064	1535 (+19.7%)	-39.8	-42.9 (0.71%)	-58.7
APNRRU [23]	1043	1328 (+3.5%)	-36.0	-38.1 (1.25%)	-58.6
<b>TRes-GRU</b>	<b>999</b>	<b>1282</b>	<b>-38.4</b>	<b>-41.2 (0.87%)</b>	<b>-59.0</b>
<b>TRes-DeltaGRU</b>	<b>999</b>	<b>1324 (+3.3%)</b>	<b>-39.6</b>	<b>-42.1 (0.79%)</b>	<b>-59.9</b>

<sup>a</sup> Percentage values indicate the difference relative to TRes-GRU.

0.001% (PAPR of 9.24 dB at CCDF of 0.01%) and sampling rate of 983.04 MHz. The dataset, consisting of 98304 samples, was split into 60% for training, 20% for validation, and 20% for testing. Additionally, the experiments were conducted on a 3.5 GHz GaN Doherty PA DUT (internal evaluation board AR211132 from Ampleon), operating at an average output power of 41.2 dBm. The PA has a P1dB compression point of 46.5 dBm, a P3dB compression point of 50 dBm, and a flat gain bandwidth of 200 MHz.

#### C. Neural Network Training

The end-to-end training process was implemented using OpenDPDv2 platform. Models were trained offline for 240 epochs using the ADAMW optimizer, configured with an initial learning rate of 5E-3, a ReduceOnPlateau decay strategy, and a batch size of 64. In the model comparison experiment, the DVR decomposition included 3 units, the PG-Just Another NETwork (JANET) model utilized a window size of 4. Both JANET models had a hidden size of 12, while the TRes-DeltaGRU model utilized 15 hidden neurons. For the temporal residual layer, the Conv1D hyperparameters are defined as  $(C_{in}, C_{out}, K, D, P)$ , where  $C_{in}$  and  $C_{out}$  represent the input and output channel sizes, respectively,  $K$  is the kernel size,  $D$  is the dilation length, and  $P$  is the padding size. The hyperparameters for the first dilated convolutional layer were set to  $(2, 3, 3, 16, 16)$ , and for the channel mixer, they were  $(3, 2, 1, 1, 1)$ . The stride of the Conv1D layer was consistently set to 1.

All experiments were performed on a single NVIDIA RTX 4090 GPU running PyTorch version 2.4.1 with CUDA version 12.4. During DPD learning, models achieving the best ACPR were saved for final evaluation.

## VI. PERFORMANCE RESULTS AND DISCUSSIONS

We evaluate the absolute linearization performance of OpenDPDv2-trained TRes-DeltaGRU DPD models of varying complexity in comparison to prior works. For giving an intuitive measure of the sparse DPD model complexity and simplified comparison, we define the number of active parameters of TRes-DeltaGRU as:

$$\begin{aligned} \text{#Active Params} = & \text{#DeltaGRU Params} \times (1 - \Gamma) \\ & + \text{#FC Params} + \text{#TCN Params} \end{aligned} \quad (18)$$

where  $\Gamma$  is temporal sparsity percentage.

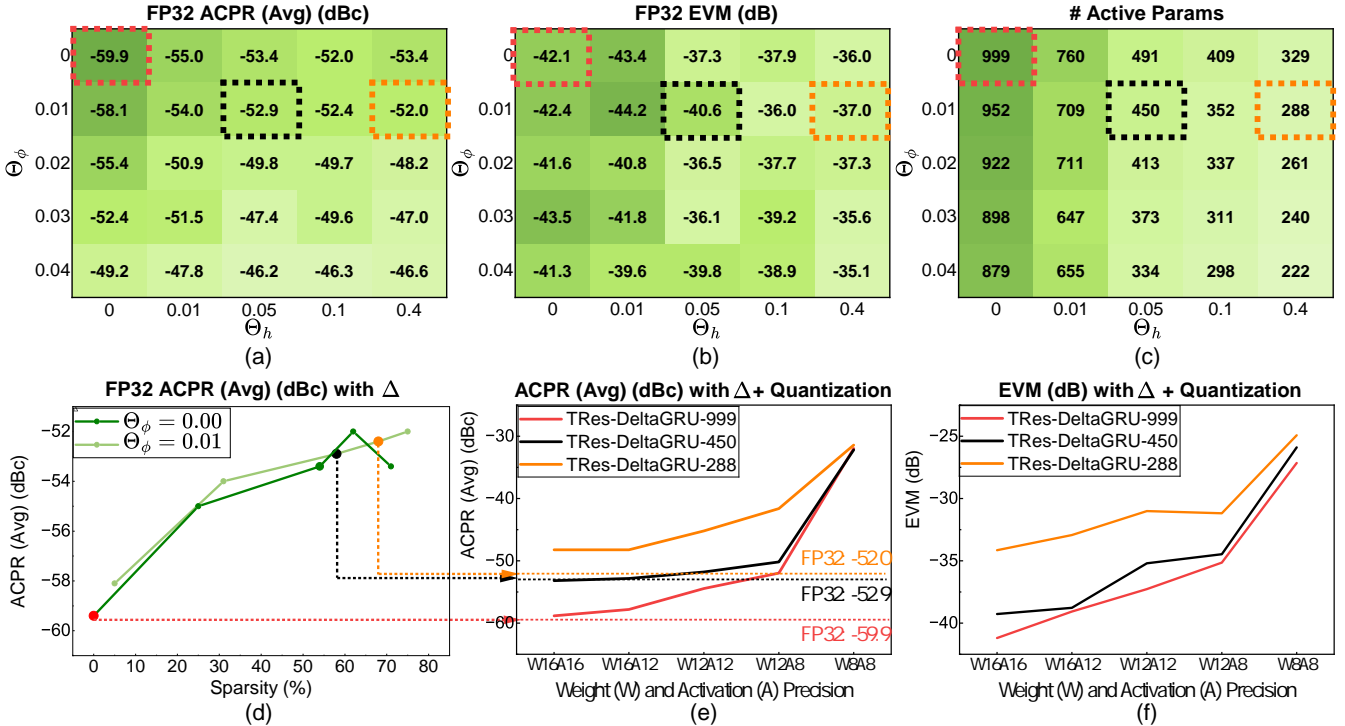


Fig. 5. Delta Threshold scan of TRes-DeltaGRU vs. (a) Average ACPR (dBc), (b) EVM (dB), (c) Number of active parameters; (d) Average ACPR (dBc) vs. sparsity with only delta. Quantization precision scan vs. (e) Average ACPR (dBc) (f) EVM (dB)

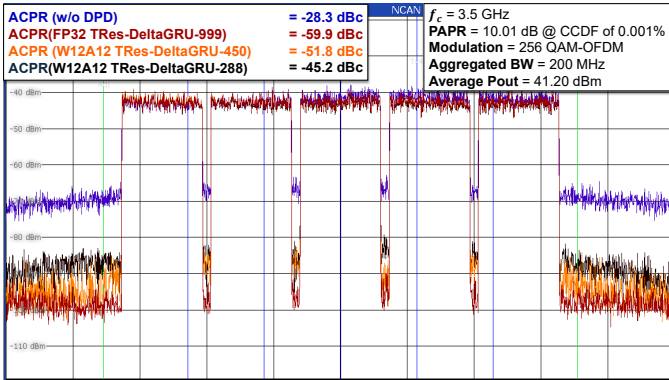


Fig. 6. Measured spectrum on the 200 MHz TM3.1a signal without DPD and with TRes-DeltaGRU DPD. A supplementary video demonstrating the spectrum analyzer configuration and the measured ACPR readouts is provided as Multimedia Extension 1 [24].

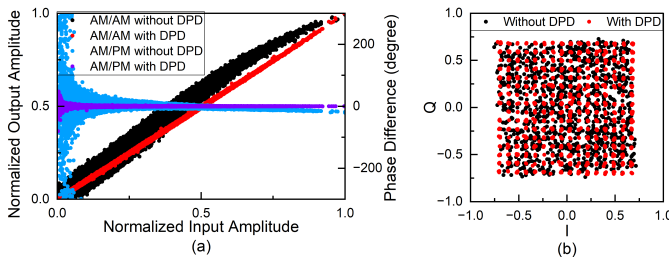


Fig. 7. (a) AM/AM and AM/PM characteristic (b) constellation on the 200 MHz TM3.1a signal without DPD and with FP32 TRes-DeltaGRU-999 DPD.

TABLE III  
ABLATION STUDY OF TEMPORALLY SPARSE DPD MODELS

DPD Model Type	Temporal Sparsity	Params #Total	Params #Active	NMSE (dB)	EVM (dB)	ACPR (dBc)
DeltaGRU	0%	1090	498	-37.1	-38.6 (1.17%)	-59.4
	56.0%			-34.9	-37.0 (1.41%)	-52.8
	75.8%			-34.6	-36.7 (1.47%)	-48.4
FCRes-DeltaGRU	0%	1094	501	-37.1	-38.4 (1.20%)	-58.0
	56.2%			-36.1	-38.2 (1.23%)	-51.4
	76.1%			-35.6	-37.0 (1.41%)	-50.1
TRes-DeltaGRU	0%	999	999	-39.8	-42.1 (0.79%)	-59.9
	56.0%			-38.1	-40.6 (0.93%)	-52.9
	72.5%			-36.0	-37.0 (1.41%)	-52.0

TABLE IV  
LINEARIZATION PERFORMANCE OF TRES-GRU (DENSE) VS. TRES-DELTAGRU (SPARSE) MODELS.

Model Type	Temporal Sparsity	Params #Total	Params #Active	Model Precision	EVM (dB)	ACPR (dBc)
Dense	-	999	999	FP32	<b>-41.2 (0.87%)</b>	-59.0
				FP32	<b>-42.1 (0.79%)</b>	-59.9
Sparse	0%	999	999	W16A16	-41.2 (0.87%)	-58.8
				W12A12	-37.3 (1.36%)	-54.5
Dense	-	524	524	FP32	<b>-37.3 (1.36%)</b>	-52.7
				FP32	<b>-40.6 (0.93%)</b>	-52.9
Sparse	56.0%	999	450	W16A16	-39.3 (1.08%)	-53.2
				W12A12	-35.2 (1.74%)	-51.8
Dense	-	311	311	FP32	<b>-34.1 (1.97%)</b>	-52.3
				FP32	<b>-37.0 (1.41%)</b>	-52.0
Sparse	72.5%	999	288	W16A16	-34.2 (1.95%)	-48.2
				W12A12	-31.0 (2.82%)	-45.2

### A. Model Comparison

Table II compares the linearization performance of the proposed TRes-DeltaGRU model with five prior state-of-the-art DPD models operating around 1000 parameters. While BO-JANET achieves the best EVM of -42.9 dB (0.71%), its ACPR of -58.7 dBc falls short of TRes-DeltaGRU's -59.9 dBc. Similarly, DVR-JANET attains the best ACPR of -59.4 dBc, it underperforms TRes-DeltaGRU in EVM (-38.6 dB/1.17% vs. -42.1 dB/0.79%). The proposed TRes-DeltaGRU model achieves balanced performance across all metrics with an Normalized Mean Square Error (NMSE) of -39.62 dB, an EVM of -42.1 dB (0.79%), and an ACPR of -59.9 dBc, demonstrating comparable linearization capability to state-of-the-art models under this test configuration.

From an energy-efficiency perspective, TRes-DeltaGRU exhibits advantages in both model size and computational cost. With 999 parameters, TRes-DeltaGRU requires fewer parameters than all compared models. Moreover, TRes-GRU has the lowest dense FLOPs among the compared models (1282). TRes-DeltaGRU incurs only a small overhead in dense FLOPs (1324, +3.3%). This computational efficiency, combined with competitive linearization performance, establishes TRes-DeltaGRU as a suitable foundation for delta-based model optimization, where reduced baseline complexity enables more effective exploitation of temporal sparsity while maintaining robust DPD performance.

### B. Ablation Study

Table III presents an ablation study comparing three DPD models with dynamic temporal sparsity: DeltaGRU without residual connections, Fully Connected Residual Delta Gated Recurrent Unit (FCRes-DeltaGRU) with a linear layer as the residual path, and TRes-DeltaGRU with a TCN residual path. The comparison reveals the critical role of the residual connection in mitigating the impact of temporal sparsity on linearization performance.

At 0% temporal sparsity, TRes-DeltaGRU achieves the best performance with an ACPR of -59.9 dBc, NMSE of -39.78 dB, and EVM of -42.12 dB (0.78%), outperforming both DeltaGRU and FCRes-DeltaGRU. The advantage of TRes-DeltaGRU becomes more evident at high sparsity levels. With around 56% sparsity, DeltaGRU shows 3.6 dB worse EVM performance than TRes-DeltaGRU while utilizing more active parameters. At sparsity levels that result in approximately 300 active parameters, TRes-DeltaGRU achieves the best high-sparsity performance among the compared delta-RNN variants, with an ACPR of -52.0 dBc. These results confirm the effectiveness of the TCN residual path.

### C. Delta Threshold Scan

Table IV demonstrates a key advantage of DPD models with dynamic temporal sparsity: by exploiting temporal sparsity, DPD models with dynamic temporal sparsity achieve superior linearization performance with fewer active parameters compared to dense models. Specifically, the

W16A16 TRes-DeltaGRU-450 model, utilizing temporal sparsity to reduce active parameters from 999 to 450, surpasses the dense FP32 TRes-GRU-524 model by 0.5 dB in ACPR and 2 dB in EVM and using 14.1% fewer active parameters (450 vs. 524). Similarly, the FP32 TRes-DeltaGRU-288 improves EVM (-37.0 dB vs. -34.1 dB), demonstrating that DPD models with dynamic temporal sparsity can achieve better DPD performance with fewer active parameters through effective exploitation of temporal sparsity. These results validate the efficacy of DPD models with dynamic temporal sparsity in achieving superior linearization with reduced computational complexity and energy consumption. Additionally, the W12A12 TRes-DeltaGRU-288 DPD model, combining temporal sparsity with quantization, meets 3GPP spectrum mask of -45 dBc and EVM standards of -30 dB with the lowest energy cost, attaining an ACPR of -45.2 dBc and an EVM of -31.0 dB.

A Delta threshold scan was conducted on a 15-hidden-neuron TRes-DeltaGRU model with varying thresholds  $\Theta_\phi$  from 0 to 0.04 and  $\Theta_h$  from 0 to 0.4. Figures 5 (a) and (b) depict the average ACPR and EVM of FP32 TRes-DeltaGRU models, while (c) illustrates the number of activated parameters. Fig. 5 (d) reflects the influence of GRU temporal sparsity on linearization performance. The TRes-DeltaGRU-999 model achieves an average ACPR of -59.9 dBc and an EVM of -42.1 dB. At higher thresholds ( $\Theta_\phi = 0.04$ ,  $\Theta_h = 0.4$ ), the number of activated parameters decreases to 222, with the FP32 TRes-DeltaGRU-222 model achieving 80.2% temporal sparsity, yielding an ACPR of -46.7 dBc and an EVM of -35.1 dB, satisfying communication standard.

### D. Model Precision Scan

Figs. 5 (e) and (f) illustrate the relationship between weight and activation precision and ACPR/EVM for the TRes-DeltaGRU DPD model with parameter counts of approximately 300, 450, and 1000. The TRes-DeltaGRU-450 model maintains an ACPR better than -45 dBc until model precision is reduced to W12A8. The trend of results shows that reduced power consumption can be attained by adopting lower precision, though this compromises accuracy.

Fig. 6 shows the screenshot of the spectrum analyzer while measuring various quantized TRes-DeltaGRU models. Fig. 7 (a) shows the AM/AM and AM/PM characteristics, and (b) shows the constellation without DPD and with FP32 TRes-DeltaGRU-999 model.

## VII. NN-BASED DPD'S POWER ANALYSIS AND DISCUSSION

While the previous sections have demonstrated the performance advantages of the proposed TRes-DeltaGRU model with dynamic temporal sparsity and quantization, practical deployment requires understanding its power consumption characteristics. This section presents a comprehensive power analysis of NN-based DPD systems, decomposing the total power consumption into inference, sampling, and adaptation components. We identify inference

power as the dominant factor and provide theoretical energy saving analysis, followed by realistic energy estimation using Gem5 simulation to validate the practical benefits of the proposed approach.

### A. NN-Based DPD's Power Issue

Figure 8 (a) illustrates the operational cycle of a practical DPD system, where periodic IQ data collection and model parameter updates (adaptation) interleave with continuous DPD inference. This cyclic operation reveals that the total power consumption of an NN-based DPD engine,  $P_{DPD}$ , can be decomposed into three principal components:

$$\begin{aligned} P_{DPD} &= P_{INF} + P_{SAM} + P_{ADA} \\ &= \frac{E_{INF}}{T_{DPD}} + \frac{E_{SAM}}{T_{DPD}} + \frac{E_{ADA}}{T_{DPD}} \end{aligned} \quad (19)$$

where:

- $T_{DPD}$ : cyclic period of DPD operation, spanning between the starting point of data sample collections from the Transmitter Observation Receiver (TOR) [8] in neighboring DPD operation cycles, which includes high-speed Analog-to-Digital Converters (ADC), down-conversion, and associated processing for online adaptation.
- $E_{INF}$ : energy consumed during DPD inference (INF), encompassing per-sample forward pass of the NN DPD model throughout  $T_{DPD}$ .
- $E_{SAM}$ : energy drawn by the TOR during IQ data sample (SAM) collection.
- $E_{ADA}$ : energy expended in updating the DPD model parameters for online adaptation (ADA).

1) *Inference Power ( $P_{INF}$ ): The Dominant Factor:* In a streaming transmitter, DPD inference operates continuously throughout  $T_{DPD}$ , processing each incoming I/Q sample at the sampling rate  $f_s$ . The inference energy consumption is fundamentally tied to the computational complexity of the NN model:

$$E_{INF} = E_F \cdot N_F = E_F \cdot f_s \cdot T_{DPD}, \quad (20)$$

where:

- $E_F$ : energy per forward pass, encompassing arithmetic operations (multiplications, additions, nonlinear activations) and memory accesses.
- $N_F$ : total number of forward passes during  $T_{DPD}$ .

Consequently, the DPD inference power consumption becomes:

$$P_{INF} = \frac{E_{INF}}{T_{DPD}} = E_F \cdot f_s \quad (21)$$

As wireless systems push toward multi-GHz sampling rates for wider bandwidths, inference power will scale proportionally and potentially reach prohibitive levels.

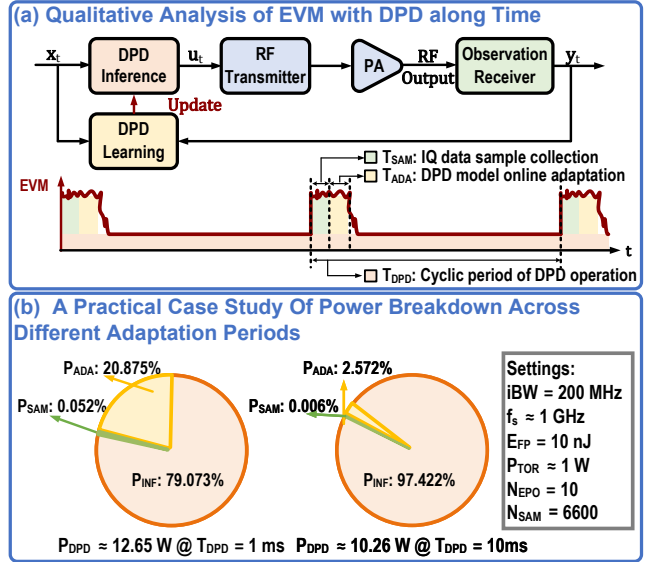


Fig. 8. (a) Qualitative Analysis of EVM with DPD vs. Time. (b) A practical case study of power breakdown across different adaptation periods.

2) *Data Collection Power ( $P_{SAM}$ ): The Periodic Overhead:* Maintaining accurate linearization requires periodic acquisition of high-quality I/Q samples from the TOR. The power contribution from this sampling process is:

$$\begin{aligned} P_{SAM} &= \frac{P_{TOR} \cdot T_{SAM}}{T_{DPD}} \\ &\approx \frac{P_{ADC} \cdot N_{SAM}}{T_{DPD} \cdot f_s}, \end{aligned} \quad (22)$$

where  $P_{TOR}$  represents the TOR's active power consumption approximating the ADC power, which is the dominant part.  $T_{SAM} = N_{SAM}/f_s$  denotes the data acquisition duration (as shown in Fig. 8 (a)), and  $N_{SAM}$  is the number of collected I/Q samples.

Notably, this component exhibits an inverse relationship with the adaptation period  $T_{DPD}$ , allowing system designers to trade off adaptation frequency against power consumption based on PA characteristics.

3) *Adaptation Power ( $P_{ADA}$ ): The Online Learning Cost:* While most existing NN-based DPD studies focus on offline implementations, practical deployments must address long-term PA variations, including thermal drift, electron trapping, and bias-point shifts that evolve over microseconds to milliseconds [25]. Online adaptation via backpropagation [26] incurs significant computational overhead, with each epoch requiring both forward (F) passes and backward (B) passes. Given that each backward pass typically requires 2–3× the computational resources of a forward pass, the adaptation power consumption can be estimated as:

$$\begin{aligned} P_{ADA} &= \frac{(E_F + E_B) \cdot N_{EPO} \cdot N_{SAM}}{T_{DPD}} \\ &\approx \frac{4E_F \cdot N_{EPO} \cdot N_{SAM}}{T_{DPD}}. \end{aligned} \quad (23)$$

where  $E_B$  is the energy per backward pass and  $N_{EPO}$  is the number of online adaptation epochs.

4) *DPD Power Breakdown: A Practical Case Study:* Synthesizing Eqs. 19, 20, 22, and 23, the total DPD power consumption becomes:

$$P_{DPD} = E_F \cdot f_s + \frac{P_{ADC} \cdot N_{SAM}}{T_{DPD} \cdot f_s} + \frac{4E_F \cdot N_{EPO} \cdot N_{SAM}}{T_{DPD}} \quad (24)$$

To ground this analysis in practical numbers, consider a TM3.1a test signal with 200 MHz baseband bandwidth sampled at 983.04 MHz (approximated to 1 GHz for clarity). Below are the assumptions:

- **Forward pass energy:**  $E_F = 10 \text{ nJ}$  per forward pass for a 1000-parameter GRU-based DPD [14];
- **Data collection:** assuming  $P_{ADC} \approx 1 \text{ W}$  for 12-bit precision at 1 GHz sample rate [27];
- **Adaptation parameters:**  $N_{EPO} = 10$  epochs,  $N_{SAM} = 6600$  samples (normalized from 2000 samples at 300 MHz [28]);
- **Update period:**  $T_{DPD}$  ranging from 1 ms to 1 s;

Figure 8 (b) presents the power breakdown across different adaptation periods. For  $T_{DPD} = 1 \text{ ms}$ , the total power consumption reaches:

$$\begin{aligned} P_{DPD} &= P_{INF} + P_{SAM} + P_{ADA} \\ &= 10.0 + 0.0066 + 2.64 = 12.65 \quad (\text{W}) \end{aligned}$$

This analysis reveals a critical insight: inference power dominates the total consumption (>79%), even with aggressive adaptation rates. For  $T_{DPD} = 10 \text{ ms}$ , the total power consumption is approximately 10.26 W. As  $T_{DPD}$  increases toward more practical values (e.g., 1 s), the inference component exceeds 99% of total power, while adaptation and sampling contributions become negligible. The reason this  $P_{DPD}$  is significantly higher than typical DPD power consumption values reported in industrial product datasheets is that we assume a completely real-time streaming large complex NN DPD operating at 1 GHz sample rate under 100% duty cycle, which does not exist in any physical product yet.

### B. Theoretical Energy Saving

Previous DPD algorithms typically assume a FP32 bit-width for active parameters when evaluating model complexity. However, the number representation format and bit-width of parameters significantly influence energy consumption during hardware implementation. For NNs, the forward pass energy consumption  $E_F$  can be expressed as:

$$E_F = E_{MUL} + E_{ADD} + E_{MEM} \quad (25)$$

where  $E_{MUL}$ ,  $E_{ADD}$ , and  $E_{MEM}$  are the total energy consumption of all multiplications (**MUL**), additions (**ADD**), and memory accesses (**MEM**) during a forward pass, respectively. When mapping from floating-point to fixed-point parameters with identical bit-width, the energy of arithmetic operations and memory access is reduced due to simpler fixed-point arithmetic hardware. For quantized fixed-point models, we define  $\alpha$  as the ratio between lower bit widths and 32 bits ( $\alpha = 0.5$  for INT16 vs. INT32). Incorporating both

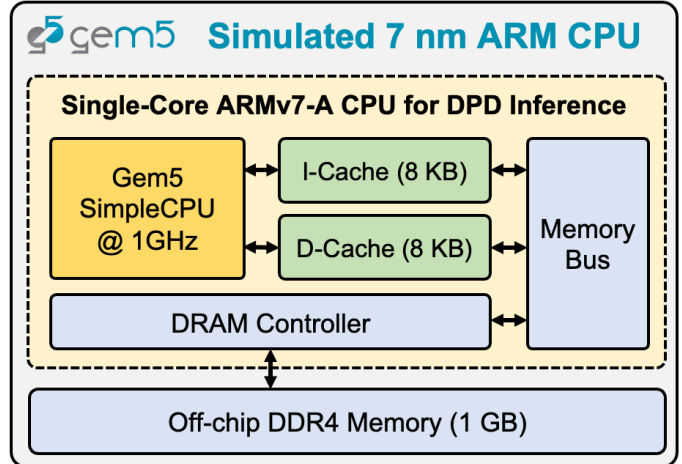


Fig. 9. Microarchitecture of the Gem5-simulated single-core CPU with the 32-bit ARMv7-A instruction set for DPD inference energy estimation under the 7 nm technology.

quantization and temporal sparsity percentage  $\Gamma$ , the operation and memory access energy numbers are given by:

$$E_{MUL} = (1 - \Gamma) \cdot \alpha^2 \cdot E_{MUL, INT32} \quad (26)$$

$$E_{ADD} = (1 - \Gamma) \cdot \alpha \cdot E_{ADD, INT32} \quad (27)$$

$$E_{MEM} = (1 - \Gamma) \cdot \alpha \cdot E_{MEM, INT32} \quad (28)$$

### C. Hardware Architecture and Simulation Setup

To validate the theoretical energy saving analysis and provide realistic energy consumption estimates that reflect real-world von Neumann architecture-based processors, this work employs the timing-accurate Gem5 [29] processor microarchitecture simulator to provide detailed statistics on instruction execution, memory hierarchy behavior, and system-level performance metrics.

1) *Simulated Microarchitecture:* The simulated processor implements a 32-bit ARM architecture targeting embedded computing scenarios suitable for DPD deployment. Fig. 9 illustrates the complete microarchitecture, featuring:

- An ARM Timing Simple CPU core using the ARMv7-A Instruction Set Architecture (ISA) with Thumb support.
- A **cache hierarchy** consists of separate L1 instruction (I-cache) and data caches (D-cache), each configured as 8KB, 4-way set-associative structures with 64-byte cache lines. We omit L2 and L3 caches to model resource-constrained embedded processors typical in the digital back-end modules in RF systems.
- A main DDR4 memory of 1GB connected to the CPU through the memory bus.

2) *Energy Modeling Framework:* The energy consumption analysis leverages detailed operation counts and memory access patterns extracted from Gem5 simulations, combined with energy characteristics of 7nm CMOS technology [18].

Energy consumption for arithmetic operations varies across data types. For FP32 operations, addition consumes 0.38 pJ while multiplication requires 1.31 pJ per operation. Integer operations exhibit quadratic scaling for multiplication and

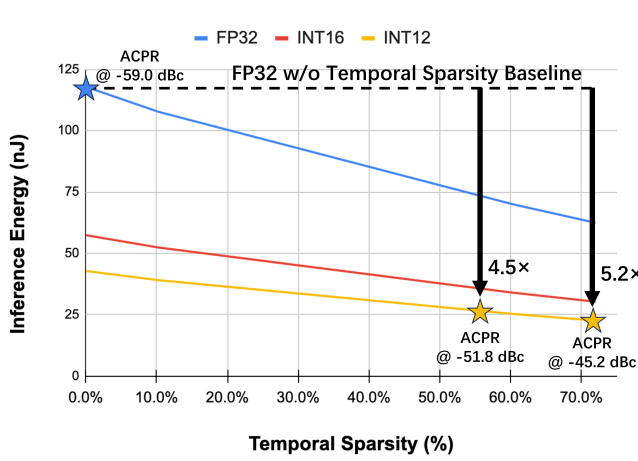


Fig. 10. TRes-DeltaGRU-999 DPD forward pass energy ( $E_F$ ) reduction with temporal sparsity estimated using the Gem5-simulated ARM CPU.

linear scaling for addition relative to bit-width. Specifically, INT16 operations consume approximately 0.015 pJ (addition) and 0.37 pJ (multiplication), while INT12 operations require 0.011 pJ (addition) and 0.21 pJ (multiplication).

Memory hierarchy energy consumption scales with both access frequency and data width. L1 cache accesses consume 7.5 pJ per access, while the DDR4 memory accesses require 1.3 nJ per transfer. The energy model incorporates data-width scaling factors: FP32 (1.0 $\times$ ), INT16 (0.5 $\times$ ), and INT12 (0.375 $\times$ ) to account for reduced data movement in quantized implementations.

3) *Simulation Configuration*: The simulation begins with cross-compilation of DPD algorithms in C programs targeting the ARMv7-A ISA. Program binaries are generated using the `arm-linux-gnueabihf-gcc` cross-compiler with optimization flags `-O3 -march=armv7-a -mfpu=neon -static` to maximum compilation optimization and make use of the NEON single-instruction-multiple-data (SIMD) vector processing unit.

During simulation, Gem5 loads the target binary into the simulated DDR4 memory and executes the DPD algorithms with an I/Q sequence length of 10,000.

#### D. Energy Analysis

This section evaluates the energy efficiency of the TRes-DeltaGRU algorithm under varying quantization precisions and temporal sparsity levels. Accurate energy estimations are provided using the Gem5-simulated ARM CPU to deliver insights critical for practical, energy-constrained RF systems. DDR4 memory energy is excluded from the analysis, as it is only utilized during initialization, and the 8KB D-cache sufficiently accommodates the entire DPD model, reflected by nearly 100% L1 cache hit rates.

Figure 10 demonstrates how forward pass energy consumption ( $E_F$ ) decreases as temporal sparsity increases in the TRes-DeltaGRU-999 DPD model. With INT12 quantization alone (no temporal sparsity), the energy is reduced by 2.8 $\times$  compared to FP32 implementations,

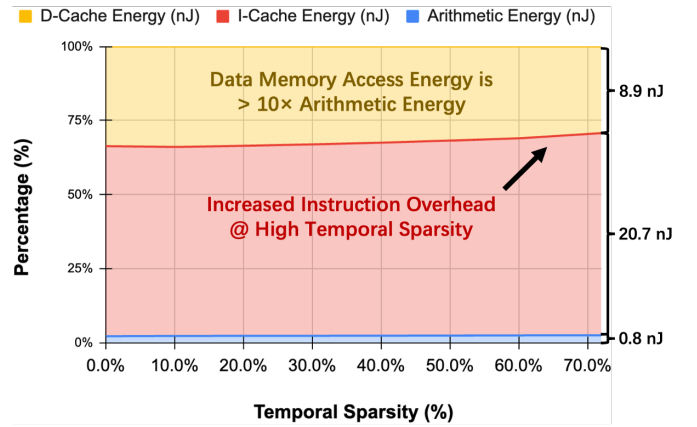


Fig. 11. TRes-DeltaGRU-999 (INT16) DPD forward pass energy breakdown on the Gem5-simulated ARM CPU.

maintaining an ACPR of -54.5 dBc. When combined with a temporal sparsity of 56.0%/72.5%, this model achieves an energy reduction factor of 4.5 $\times$ /5.2 $\times$ , while still meeting a common ACPR target of -45 dBc. These results confirm OpenDPDv2's effectiveness in significantly decreasing energy demands without compromising critical linearization performance.

Figure 11 provides a breakdown of forward pass energy consumption for the TRes-DeltaGRU-999 DPD model operating at INT16 precision across different sparsity levels. A key insight is that memory access dominates overall energy consumption as D-cache energy alone surpasses arithmetic operation energy by more than an order of magnitude. Consequently, future hardware implementations should prioritize reducing memory access through joint algorithmic and circuit-level optimizations, emphasizing algorithm-hardware co-design [30]. Furthermore, Figure 11 also reveals that increased temporal sparsity leads to a higher relative proportion of I-cache energy consumption, attributed to overhead operations such as delta vector encoding, memory updates, and indexing. While this overhead can diminish the benefits of sparsity in general-purpose CPUs, a specialized ASIC implementation can effectively mitigate these inefficiencies, further enhancing energy savings.

The absolute energy numbers evaluated by Gem5 are overall significantly larger than the rough estimation reported in [13], [14], which is because prior works assumed 100% reuse of operands in an ideal multiply-and-accumulate array without overhead. In contrast, our Gem5-based analysis incorporates realistic processor behaviors and overheads associated with general-purpose 32-bit instruction set architectures. Therefore, the sum of arithmetic and D-cache energy values will provide a more accurate benchmark for potential ASIC implementations.

#### E. Implications for Power-Efficient Wideband DPD Design

As demonstrated by the power breakdown analysis, inference power dominates total consumption and scales linearly with model complexity and sampling rate. The theoretical and experimental results presented in this section confirm that the primary path towards energy-efficient NN

DPD lies in aggressively reducing  $E_F$  through model compression techniques. In this work, we integrate DPD learning and optimization through model quantization and temporal sparsification to reduce DPD forward pass complexity, which contributes to the reduction of  $P_{\text{INF}}$  and  $P_{\text{ADA}}$ . The Gem5 simulation results validate that our approach achieves significant energy savings (up to  $5.2\times$  reduction) while maintaining robust linearization performance. Complementary strategies for further energy reduction include dedicated hardware accelerators on FPGAs [31] or ASICs [32], low-sampling-rate DPD [7], and sub-Nyquist TOR techniques [33].

### VIII. CONCLUSION

This paper presents OpenDPDv2, an end-to-end framework that streamlines NN-based DPD learning and deployment-oriented optimization with standardized datasets and reproducible baselines. We also propose TRes-DeltaGRU, which introduces a TCN-based temporal residual path to improve robustness under aggressive delta thresholds and enables joint optimization with temporal sparsity and quantization-aware training. Measured on a 200-MHz TM3.1a OFDM signal at 41.2 dBm average output power, FP32 TRes-DeltaGRU-999 achieves -59.9 dBc ACPR and -42.1 dB EVM. Gem5-based energy analysis further shows that mixed precision and temporal sparsity can reduce forward pass energy by up to  $5.2\times$  while meeting a -45 dBc ACPR target. These results highlight TRes-DeltaGRU and OpenDPDv2 as practical building blocks for power-efficient wideband NN-DPD.

### ACKNOWLEDGMENT

We thank Yi Zhu and John Gajadharsing from Ampleon for lending us the PA DUT and assistance in building the experimental setup. We also thank Prof. Leo C. N. de Vreede from Delft University of Technology and Prof. Anding Zhu from University College Dublin for related technical discussions and writing suggestions. This work is partially supported by the European Research Executive Agency (REA) under the Marie Skłodowska-Curie Actions (MSCA) Postdoctoral Fellowship program, Grant No. 101107534 (AIRHAR).

### REFERENCES

- [1] “3gpp specification series,” Available at <https://www.3gpp.org/dynareport?code=38-series.htm>.
- [2] T. Kobal, Y. Li, X. Wang, and A. Zhu, “Digital predistortion of RF power amplifiers with phase-gated recurrent neural networks,” *IEEE Trans. Microw. Theory Techn.*, vol. 70, no. 6, p. 3291–3299, Jun 2022.
- [3] T. Kobal and A. Zhu, “Digital predistortion of RF power amplifiers with decomposed vector rotation-based recurrent neural networks,” *IEEE Trans. Microw. Theory Techn.*, vol. 70, no. 11, p. 4900–4909, Nov 2022.
- [4] A. Fischer-Bühner, L. Anttila, M. Dev Gomony, and M. Valkama, “Recursive neural network with phase-normalization for modeling and linearization of rf power amplifiers,” *IEEE Microwave and Wireless Technology Letters*, vol. 34, no. 6, pp. 809–812, 2024.
- [5] Q. Zhang, C. Jiang, G. Yang, R. Han, and F. Liu, “Block-oriented recurrent neural network for digital predistortion of rf power amplifiers,” *IEEE Transactions on Microwave Theory and Techniques*, vol. 72, no. 7, pp. 3875–3885, 2024.
- [6] S. Wesemann, J. Du, and H. Viswanathan, “Energy efficient extreme mimo: Design goals and directions,” *IEEE Communications Magazine*, vol. 61, no. 10, pp. 132–138, 2023.
- [7] Y. Li, X. Wang, and A. Zhu, “Sampling rate reduction for digital predistortion of broadband RF power amplifiers,” *IEEE Trans. Microw. Theory Techn.*, vol. 68, no. 3, pp. 1054–1064, 2020.
- [8] N. Hammler, A. Cathelin, P. Cathelin, and B. Murmann, “A spectrum-sensing dpd feedback receiver with  $30\times$  reduction in adc acquisition bandwidth and sample rate,” *IEEE Transactions on Circuits and Systems I: Regular Papers*, vol. 66, no. 9, pp. 3340–3351, 2019.
- [9] Y. Li, X. Wang, and A. Zhu, “Reducing power consumption of digital predistortion for RF power amplifiers using real-time model switching,” *IEEE Trans. Microw. Theory Techn.*, vol. 70, no. 3, pp. 1500–1508, 2022.
- [10] M. Beikmirza, L. C. de Vreede, and M. S. Alavi, “A low-complexity digital predistortion technique for digital i/q transmitters,” in *2023 IEEE/MTT-S International Microwave Symposium - IMS 2023*, 2023, pp. 787–790.
- [11] Z. Liu, X. Hu, L. Xu, W. Wang, and F. M. Ghannouchi, “Low computational complexity digital predistortion based on convolutional neural network for wideband power amplifiers,” *IEEE Transactions on Circuits and Systems II: Express Briefs*, vol. 69, no. 3, pp. 1702–1706, 2022.
- [12] Y. Wu, G. D. Singh, M. Beikmirza, L. C. N. de Vreede, M. Alavi, and C. Gao, “OpenDPD: An Open-Source End-to-End Learning & Benchmarking Framework for Wideband Power Amplifier Modeling and Digital Pre-Distortion,” *arXiv preprint arXiv:2401.08318*, 2024.
- [13] Y. Wu, A. Li, M. Beikmirza, G. D. Singh, Q. Chen, L. C. N. de Vreede, M. Alavi, and C. Gao, “MP-DPD: Low-complexity mixed-precision neural networks for energy-efficient digital predistortion of wideband power amplifiers,” *IEEE Microwave and Wireless Technology Letters*, pp. 1–4, 2024.
- [14] Y. Wu, Y. Zhu, K. Qian, Q. Chen, A. Zhu, J. Gajadharsing, L. C. N. de Vreede, and C. Gao, “DeltaDPD: Exploiting dynamic temporal sparsity in recurrent neural networks for energy-efficient wideband digital predistortion,” *IEEE Microwave and Wireless Technology Letters*, pp. 1–4, 2025.
- [15] H. Duan, M. Versluis, Q. Chen, L. C. N. de Vreede, and C. Gao, “TCN-DPD: Parameter-efficient temporal convolutional networks for wideband digital predistortion,” 2025. [Online]. Available: <https://arxiv.org/abs/2506.12165>
- [16] D. Neil, J. H. Lee, T. Delbruck, and S.-C. Liu, “Delta networks for optimized recurrent network computation,” in *International conference on machine learning*. PMLR, 2017, pp. 2584–2593.
- [17] M. Horowitz, “1.1 computing’s energy problem (and what we can do about it),” in *2014 IEEE international solid-state circuits conference digest of technical papers (ISSCC)*. IEEE, 2014, pp. 10–14.
- [18] N. P. Jouppi, D. H. Yoon, M. Ashcraft, M. Gottscho, T. B. Jablin, and K. G. et al, “Ten lessons from three generations shaped google’s TPUv4i: Industrial product,” in *2021 ACM/IEEE 48th Annual International Symposium on Computer Architecture (ISCA)*. IEEE, 2021, pp. 1–14.
- [19] M. Nagel, M. Fournarakis, R. A. Amjad, Y. Bondarenko, M. van Baalen, and T. Blankevoort, “A white paper on neural network quantization,” *CoRR*, vol. abs/2106.08295, 2021. [Online]. Available: <https://arxiv.org/abs/2106.08295>
- [20] Y. Bengio, N. Léonard, and A. Courville, “Estimating or propagating gradients through stochastic neurons for conditional computation,” *arXiv preprint arXiv:1308.3432*, 2013.
- [21] R. . Schwarz, “Understanding basic spectrum analyzer operation.” [Online]. Available: [https://www.rohde-schwarz.com/us/products/test-and-measurement/essentials-test-equipment/spectrum-analyzers/understanding-basic-spectrum-analyzer-operation\\_256005.html](https://www.rohde-schwarz.com/us/products/test-and-measurement/essentials-test-equipment/spectrum-analyzers/understanding-basic-spectrum-analyzer-operation_256005.html)
- [22] P. Jaraut, M. Rawat, and F. M. Ghannouchi, “Composite neural network digital predistortion model for joint mitigation of crosstalk, i/q imbalance, nonlinearity in mimo transmitters,” *IEEE Trans. Microw. Theory Techn.*, vol. 66, no. 11, pp. 5011–5020, Nov 2018.
- [23] A. Fischer-Bühner, L. Anttila, M. Turunen, M. Dev Gomony, and M. Valkama, “Augmented phase-normalized recurrent neural network for rf power amplifier linearization,” *IEEE Transactions on Microwave Theory and Techniques*, vol. 73, no. 1, pp. 412–422, 2025.
- [24] Chang Gao, “OpenDPDv2 Measurement Demo by Yizhuo Wu,” Dec. 2025. [Online]. Available: <https://youtu.be/n3765lm3QZI>
- [25] A. Fischer-Bühner, L. Anttila, A. Brihuega, M. Dev Gomony, and M. Valkama, “Predistortion of gan power amplifier transient responses in time-division duplex using machine learning,” *IEEE Microwave and Wireless Technology Letters*, vol. 35, no. 6, pp. 924–927, 2025.

- [26] D. E. Rumelhart, G. E. Hinton, and R. J. Williams, “Learning representations by back-propagating errors,” *nature*, vol. 323, no. 6088, pp. 533–536, 1986.
- [27] Texas Instruments, “ADC12SJ1600 12-Bit, 1.6-GSPS, RF-Sampling Analog-to-Digital Converter (ADC),” [https://www.ti.com/lit/ds/symlink/adc12sj1600.pdf?ts=1751638711567&ref\\_url=https%253A%252F%252Fwww.ti.com%252Fdata-converters%252Fadc-circuit%252Fproducts.html](https://www.ti.com/lit/ds/symlink/adc12sj1600.pdf?ts=1751638711567&ref_url=https%253A%252F%252Fwww.ti.com%252Fdata-converters%252Fadc-circuit%252Fproducts.html), May 2025, accessed: Jul. 4, 2025.
- [28] Y. Li, X. Wang, and A. Zhu, “Complexity-reduced model adaptation for digital predistortion of rf power amplifiers with pretraining-based feature extraction,” *IEEE Transactions on Microwave Theory and Techniques*, vol. 69, no. 3, pp. 1780–1790, 2021.
- [29] J. Lowe-Power, A. M. Ahmad, A. Akram, M. Alian, R. Amslinger, M. Andreozzi *et al.*, “The gem5 simulator: Version 20.0+,” 2020. [Online]. Available: <https://arxiv.org/abs/2007.03152>
- [30] S.-C. Liu, C. Gao, K. Kim, and T. Delbruck, “Energy-efficient activity-driven computing architectures for edge intelligence,” in *2022 International Electron Devices Meeting (IEDM)*, 2022, pp. 21.2.1–21.2.4.
- [31] M. Versluis, Y. Wu, and C. Gao, “Sparsedpd: A sparse neural network-based digital predistortion fpga accelerator for rf power amplifier linearization,” 2025. [Online]. Available: <https://arxiv.org/abs/2506.16591>
- [32] A. Li, H. Wu, Y. Wu, Q. Chen, L. C. N. de Vreede, and C. Gao, “Dpd-neuralengine: A 22-nm 6.6-tops/w/mm<sup>2</sup> recurrent neural network accelerator for wideband power amplifier digital pre-distortion,” in *2025 IEEE International Symposium on Circuits and Systems (ISCAS)*, 2025, pp. 1–5.
- [33] N. Hammel, *Sub-Nyquist Receiver for Digital Predistortion of RF Power Amplifiers*. Stanford University, 2019.



**Chang Gao** (Member, IEEE) received his Ph.D. degree with Distinction in Neuroscience from the Institute of Neuroinformatics, University of Zürich and ETH Zürich, Zürich, Switzerland, in March 2022 and his master degree from Imperial College London in September 2016 and his bachelor degree from University of Liverpool and Xi'an Jiaotong-Liverpool University in July 2015. Since August 2022, he has been an assistant professor in the Department of Microelectronics at TU Delft, The Netherlands, where he leads the Lab of Efficient Machine Intelligence (EMI), focusing on neuromorphic algorithm-hardware co-design for edge AI computing. He received the 2022 Misha Mahowald Early Career Award in Neuromorphic Engineering and the 2022 Marie-Curie Postdoctoral Fellowship. He is a 2023 Dutch Research Council (NWO) Veni laureate and a 2023 MIT Technology Review Innovator Under 35 in Europe for his contribution to algorithm-hardware co-design for efficient sparse recurrent neural network edge computing.



**Yizhuo Wu** (Graduate Student Member, IEEE) obtained her M.Sc. degree in Microelectronics at TU Delft in 2023. She is now a PhD student supervised by Dr. Chang Gao in the Lab of Efficient Circuits & systems for Machine Intelligence (EMI). Her research focuses on software-hardware co-designed AI for I/Q signal processing, which aims to find energy-efficient solutions for high-frequency signal processing tasks.



**Ang Li** (Graduate Student Member, IEEE) received the B.S. degree in Microelectronics from the School of Microelectronics, Xidian University, Xi'an, China, in 2019, and the M.S. degree in Integrated Circuits from the School of Integrated Circuits, Tsinghua University, Beijing, China, in 2022. He is currently pursuing a Ph.D. in the Department of Microelectronics at Delft University of Technology, The Netherlands. His research interests include deep learning, digital circuit design, computer vision, and VLSI digital signal processing.